Front. Optoelectron. 2021, 14(3): 352–359
https://doi.org/10.1007/s12200-020-0964-8

RESEARCH ARTICLE

Characteristics of laser induced discharge tin plasma and its extreme ultraviolet radiation

Junwu WANG (✉), Xinbing WANG, Duluo ZUO

Wuhan National Research Center for Optoelectronics, Huazhong University of Science and Technology, Wuhan 430074, China

Abstract In this paper, a CO_2 laser induced discharge plasma extreme ultraviolet (EUV) source experimental device was established. The optical emission spectroscopy was used to diagnose the characteristics of the plasma, and the evolution of electron temperature and electron density with time was obtained. The influence of discharge voltage on plasma parameters was analyzed and discussed. The EUV radiation characteristics of the plasma were investigated by self-made grazing incidence EUV spectrometer. The EUV radiation intensity and conversion efficiency were discussed.

Keywords extreme ultraviolet (EUV) radiation, laser induced discharge plasma, optical emission spectroscopy, electron temperature and density

1 Introduction

The pulsed CO_2 laser produced tin droplet plasma extreme ultraviolet (EUV) sources will be used in high volume manufacturing (HVM) in semiconductor industry [1]; the demand for mask inspection and spectral metrology EUV sources has also increased [2]. At present, the EUV light source technology for lithography requires that the micron-sized tin droplet target [3] must be highly synchronized with the pre-pulse and the main pulse in time and space [4], resulting in a relatively complicated technique and not suitable for measurement and mask inspection [5]. Discharge produced plasma (DPP) EUV sources have the potential use in mask inspection application with higher wall-plug efficiency and simple structure. After years of research, DPP light source has developed into a laser induced discharge plasma (LDP) light source [6]. Since 2003, Phillips and XTREME Technologies GmbH [7] set up a new kind of LDP source, LDP has made great progress especially after using the Sn-coated rotating disc electrodes [8]. LDP combines the advantages of high stability of DPP and power scalability of laser-produced plasma (LPP) [9]. It shows properties of high brightness, simple structure and low cost [10], and becomes a promising technology in the fields of mask inspection [11] and spectral metrology [12,13]. In 2014, Ushio [14] achieved a peak brightness of 145 W/(mm^2·sr) using Sn LDP EUV source. In 2017, the peak brightness reached 225 W/(mm^2·sr) and an average brightness of 145 W/(mm^2·sr) was obtained at a maximum discharge frequency of 9.5 kHz [15].

The optical spectrum characterization of laser induced discharge plasma can provide information on the plasma ionization balance, rate processes and the density and temperature, while optical emission spectrometry (OES) is an effective and simple way to obtain the plasma parameter. OES has good space-time resolution and measurement reliability. It has been used to investigate the laser produced Sn plasma EUV source for many years. In 2010, Shaikh et al. [16] showed the electron temperature and electron density from Sn plasma produced by a CO_2 laser would be lower than the results using a neodymium-doped yttrium aluminum garnet laser in a similar parameter regime. In 2013, Wu et al. [17] measured the spectral, spatial, and temporal emission characteristic of tin LPP. However, few works had been done to the analysis of the discharge produced plasma characteristics of Sn target. In 2004, Kieft et al. [18,19] presented time-resolved measurements of Stark broadened linewidth in a pulsed tin discharge experiment and recorded the variations of the four Sn III lines from 522 to 533 nm. They found the electron density increased from 10^{23} m^{-3} before discharge to 10^{24} m^{-3} after discharge began and decreased to 10^{22} m^{-3} during the decay of plasma. In 2011, Zhu et al. [20] used a modified Stark broadening method to investigate the spatial-resolved evolutions of electron temperature and density after the maximum implosion of discharge. In

Received September 16, 2019; accepted December 23, 2019

E-mail: wjw1546112421@163.com

2014, Tobin [21] presented his optical and EUV studies of laser triggered *Z*-pinch discharge which showed a temperature of about 6.1 eV and a density of 8.3 × 10^{18} cm^{-3} at a delay time following the maximum discharge current.

In this paper, we presented a complete analysis of the optical emission features of CO_2 laser induced discharge tin plasma, and time-resolved measurements of the emission spectrums of plasma in visible spectral regions have been observed. The relation of lines intensity with discharge voltage has been investigated. Line intensities from the same ionization stage of Sn species are used in the Boltzmann plot for determining electron temperature, while electron densities are calculated using the Stark broadening method. The temporal evolution of electron temperature and density at different discharge voltage has been analyzed. The EUV spectrums of various discharge voltage were obtained.

2 Experimental details

The experimental device is shown in Fig. 1, and the vacuum chamber maintained the pressure at 1 × 10^{-3} Pa by mechanical pump and turbo pump. A stainless steel cone is used as the anode. Its angle was 60° and bottom diameter was 10 mm. The cathode was a tin disc with 4 cm in diameter and 3 mm in thickness. The discharge current was sustained with a 250 nF capacitor. The voltage varied from 0 to 17 kV. The gap between two electrodes was 6 mm.

The energy of the pulsed CO_2 laser was about 145 mJ, the full width at half maxima (FWHM) of the pulse was 90 ns and the repetition rate was 1 Hz. Laser was focused on the cathode surface through a lens with focal length of 150 mm, the diameter of spot size was 300 μm and the maximum power density was 3 GW/cm^2. An initial plasma produced by laser caused the breakdown between two electrodes. The voltage between electrodes was measured by a high voltage probe (Tektronix P6015A, × 1000, 3.0 pF, 100 MΩ) and the current was measured by a current monitor (Pearson 4997, 0.01 Volts/Amp), both were connected to the oscilloscope.

A visible spectrometer (Acton, SpectraPro-2750) was perpendicular to the discharge axis and collected the visible spectra radially produced by the plasmas. The spectrometer with a grating groove density of 300 lines/mm was connected to an intensified charge-coupled device (ICCD) camera (Princeton Instrument, PI-MAX-1300). It can realize the digital accurate scanning in the wavelength range of 300−700 nm and the spectral resolution was 0.088 nm.

The camera gate was set to 10 ns and the delay interval was set to 100 ns. The laser signal was detected by a photodiode to trigger the ICCD camera. With different delays, the visible spectra at different stages of discharge were obtained. A standard spectral lamp was used to calibrate the wavelength, there was a relationship between the spectra wavelength λ' and the number of CCD cells X, as shown in Eq. (1). Some characteristic spectral lines were found in the NIST database (Hg 546.08, 576.96,

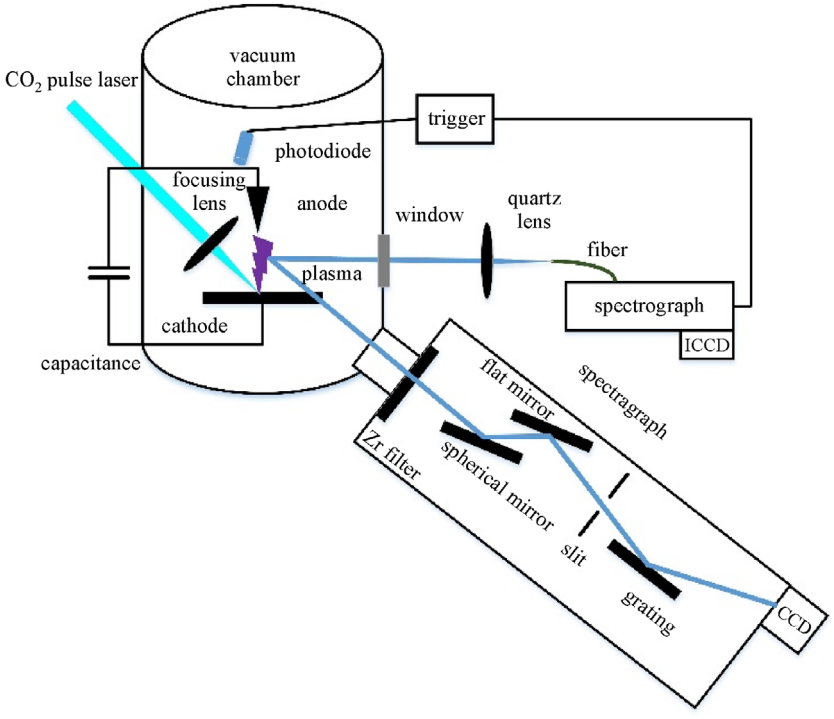

Fig. 1 LDP OES and EUV spectra detection experimental setup

579.07 nm, etc.), and the coefficients A, B and C could be determined.

$$\lambda' = A + BX + CX^2. \quad (1)$$

And a tungsten lamp was used to find out the spectral responsivity η', as shown in Eq. (2). Here $I_{measured}$ was the measured intensity and I_{lamp} was the standard intensity offered by the product manual at each wavelength.

$$\eta' = I_{measured}/I_{lamp}. \quad (2)$$

An EUV spectrometer was perpendicular to the discharge axis. The spectrometer consisted of a zirconium (Zr) film, a spherical reflector, a planar mirror, a slit, a variable pitch concave grating, a thermoelectrically cooled back-illumination X-ray CCD camera (Princeton Instruments-SX:400) and the vacuum system. The thickness of Zr film was 500 nm. Its transmittance was about 20% in the wavelength range from 6 to 18 nm. Suppose λ is the wavelength of the light to be measured, the diffraction angle is β, d is the grating constant, $\alpha = 87°$ is the incident angle, and $m = 1$ is the diffraction order. According to the grating Eq. (3),

$$d(\sin\alpha - \sin\beta) = m\lambda. \quad (3)$$

Here the position on the CCD is x, and L is the distance between the grating and the CCD plane. We can get Eq. (4).

$$\lambda = d\left\{\sin 87° - \sin\left[\operatorname{arccot}\left(\cot\beta + \frac{x - x_0}{L}\right)\right]\right\}. \quad (4)$$

As long as the relative positions of the unknown spectral line λ and the known spectral line λ_0 on the CCD were determined, the wavelengths could be calibrated. The X-ray less than 6 nm was almost absorbed by Zr film, and a sharp absorption boundary could be formed at 6 nm, so the calibration could be realized through the position of absorption boundary x_0.

3 Results and discussion

3.1 Emission spectroscopy diagnosis

When the voltage was 8.0 kV, the waveforms of discharge voltage and current were shown in Fig. 2(a); the electrodes

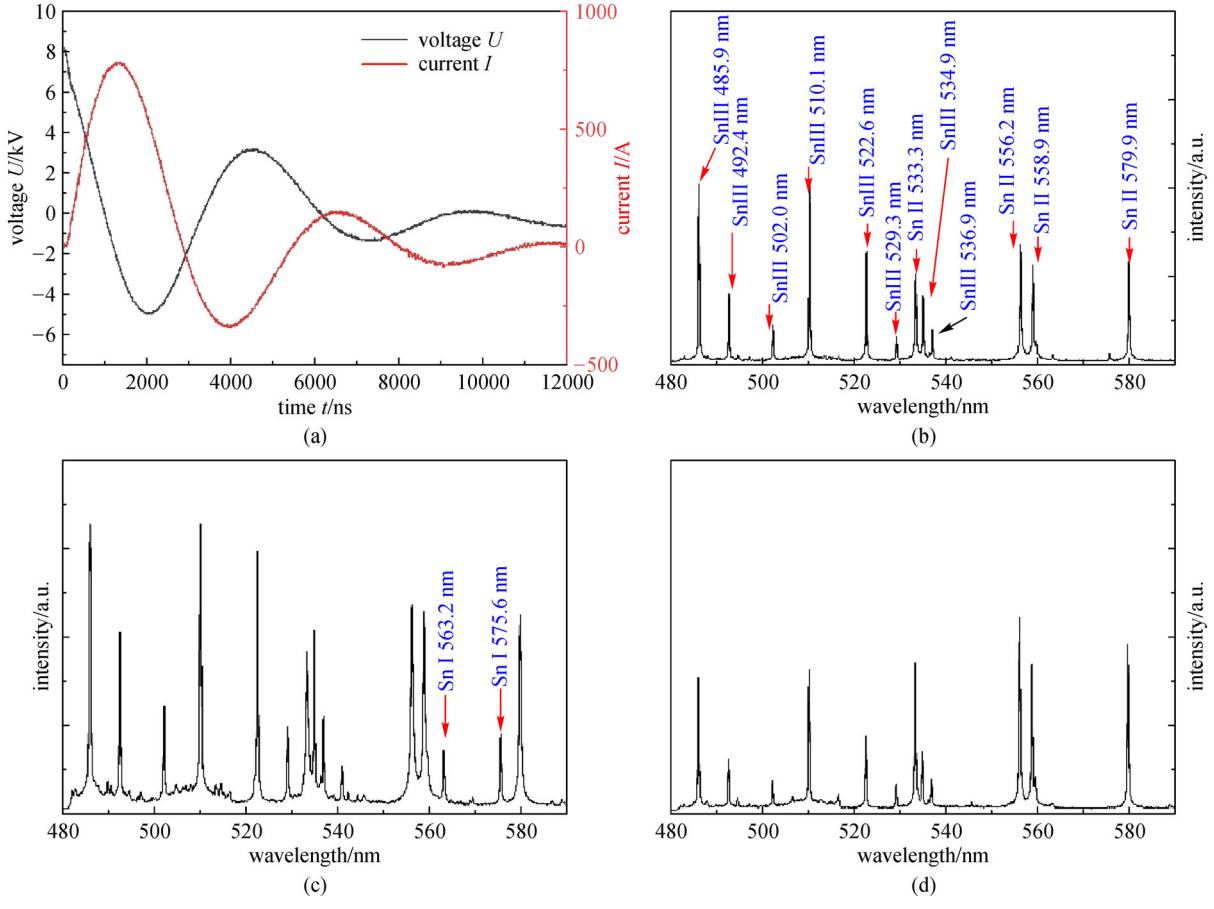

Fig. 2 (a) Waveforms of the discharge voltage and current; and laser induced discharge visible spectra at different times: (b) 200 ns; (c) 800 ns; (d) 2000 ns

breakdown occurred at 0 ns, then the voltage dropped to zero after about 1000 ns and the current reached the first peak after about 1350 ns. The 300 lines/mm grating was chosen, and 535 nm was selected as the central wavelength. The OESs of 480–590 nm were shown in Figs. 2(b)–2(d) corresponding to the spectra at different times during the discharge. The visible light lines mainly came from neutral (563.17, 575.36 nm, etc.), singly ionized (533.39, 556.19, 558.89, 579.92 nm, etc.) and doubly ionized tin (522.6, 529.3, 535.1, 537.1 nm, etc.) [22]. From 200 to 800 ns, the current increased and tin emission lines became stronger due to the ablation of target and joule heat heating, especially the intensities of Sn III lines. New tin atomic spectra lines such as Sn I 563.2 and 575.6 nm appeared apparently due to the recombination of high valence ions. From 800 to 2000 ns, tin emission lines became weaker with the decrease of current, and the new tin atomic spectra lines disappeared again. Intensities of the Sn III lines decreased more than that of the Sn II lines. With the decrease of current, fewer Sn particles were supplied, and the plasma expanded which induced large quantities of high valence ions lost energy and returned to the low valence states.

With different voltages, the LDP spectra were shown as Fig. 3. 800 ns after the discharge, the LDP spectra emission lines with higher voltage owned stronger intensities and wider broadening. The differences of singly ionized tin lines broadenings and shifts were more obvious than that of the doubly ionized tin lines and atomic tin lines. According to the widely used semi-empirical equations advanced by Griem [23], the Stark widths and the absolute value of line shifts are related with electron temperature and density.

Here we assumed the plasma was in the local thermal equilibrium (LTE), so the numbers of Sn atoms and ions in different states satisfied the Boltzmann distribution, and the electron density and the ion density satisfied the Saha equation. Considering two lines at the same charge states, the electron temperature was estimated by the Boltzmann plot, shown as Eq. (5) [24]. The differences of excitation energies should be large enough to ensure the accuracy of electron temperature, here five lines of Sn II: 556.19, 558.89, 579.92, 645.35 and 684.40 nm were chosen. When the voltage was 8.0 kV, the Boltzmann plot was shown in Fig. 4(a).

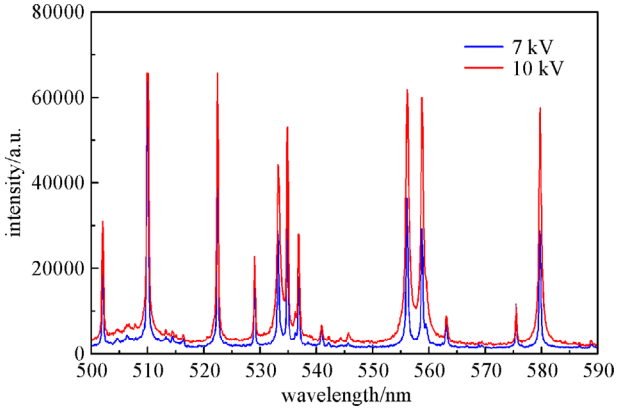

Fig. 3 LDP visible spectra with different voltages

$$\ln\left(\frac{I_1\lambda_1}{A_1g_1}\right)-\ln\left(\frac{I_2\lambda_2}{A_2g_2}\right)=-\frac{E_1-E_2}{k_{\mathrm{B}}T_{\mathrm{e}}}. \tag{5}$$

Here I_i was the intensity of the line, g_i was the energy level degeneracy, A_i was the transition probability, E_i was the excitation energy of the upper level, k_{B} was the Boltzmann constant. The black dots represented the experimental data and the red line was the linear fitting plot, the slope of the fitting line reflected the electron temperature. At 500 ns, the electron temperature was about 2.1 eV.

The electron temperatures were shown in Fig. 4(b). In the first 300 ns, the electron temperature dropped a little bit due to the dissipation of laser plasma and the incomplete development of discharge plasma. Then the electron temperature reached the peak at about 1400 ns and then decreased after the current peak.

When the voltage was 15.0 kV, at 900 ns, the Voigt fitting of Sn II 579.92 nm line is shown in Fig. 5(a). The relationship between the FWHM of a Stark-broadened line and the electron density is given by Eq. (6) [25], where W was the electron-impact parameter [26].

$$\Delta\lambda_{1/2}=2W\left(\frac{n_{\mathrm{e}}}{10^{16}}\right). \tag{6}$$

The variation of electron density was shown in Fig. 5(b). The lines represented the currents, and the dots represented the electron densities when the voltages were 8 and 15 kV. The variation trend of electron density was similar to that of the electron temperature, except that the density reached maximum not exactly the moment of current peak but a few hundred nanoseconds earlier. It could be explained by the construction of plasmas. After the breakdown, the diameter of the plasma column varied with the current. The variation of the diameter was influenced by the plasma thermal expansion pressure and the magnetic compression pressure. In the beginning, the expansion pressure was greater than the magnetic compression pressure, the plasma expanded. With the increase of current, the magnetic compression pressure became greater than the expansion pressure, the pinch of plasma appeared before the current reached the maximum. And the moment of maximum density might appear after the pinch of plasma [27].

With the known electron temperatures and densities, an approximate Eq. (7) [28] could be used to estimate the average ionized state Z, the constant D was 4.8×10^{24} cm^{-3}(10^6 K)$^{-3/2}$, Z_0 was the atomic number, here Z_0 = 50 for tin.

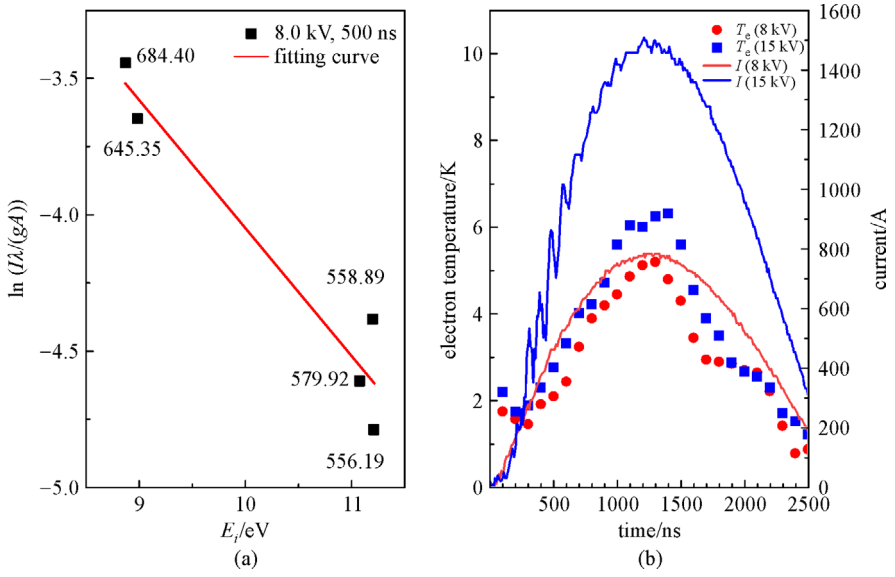

Fig. 4 (a) Boltzmann plot for electron temperature calculating; (b) electron temperatures and current waveforms versus time under different condition of discharge voltage

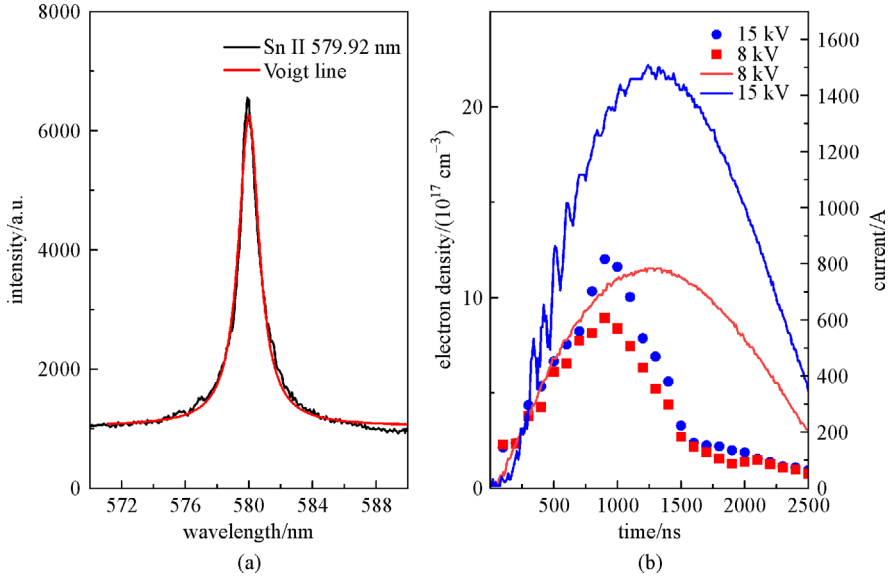

Fig. 5 (a) Voigt line fitting of Stark broadening for electron density calculating; (b) electron densities and current waveforms versus time under different condition of discharge voltage

$$Z = Z_0\left\{1-\exp\left[-4.115\left(\frac{T_e}{Z_0^{\frac{4}{3}}}\ln\frac{DT_e^{\frac{3}{2}}}{n_e}-1.16\times10^{-4}\right)^{0.625}\right]\right\}-0.5. \quad (7)$$

The average ionized states were influenced by electron temperature and density, however the electron temperature seemed to play a major role. As shown in Fig. 6, the average ionized state reached its maximum during the current peak. A higher average ion charge state meant more Sn^{7+-13+} ions were produced which meant the strongest EUV radiation was at the moment of maximum current. A higher voltage brought plasma with a higher average ionized state, which facilitated the generation of EUV in 13.5 nm.

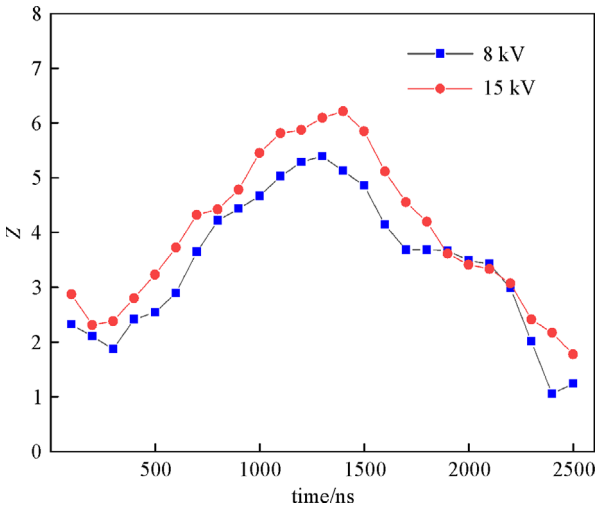

Fig. 6 Average ionized states with different voltages

3.2 LDP EUV spectra

The LPP EUV spectra were not obtained with only laser and without discharge voltages. The LDP EUV spectra at different discharge voltages from 7 to 17 kV were shown in Fig. 7. The *Y* axis units were the X-ray CCD counts which represented the relative intensity. When the voltage was higher than 7 kV, the spectra began to exhibit a strong peak between 13 to 14 nm. With the increase of voltage, the EUV intensity increased. The relationship of EUV spectral integral intensity and injected energy was plotted as shown in Fig. 8. The total discharge energy was equal to $0.5CU^2$, here C was the capacitance and U was the voltage. The spectral intensity means the integral intensity of spectrum in 13.5 nm with 2% bandwidth which represented the relative strength of EUV. With the increase of energy from 0.8 to 10.2 J, the integral intensity increased almost linearly. It showed that the EUV emission was closely

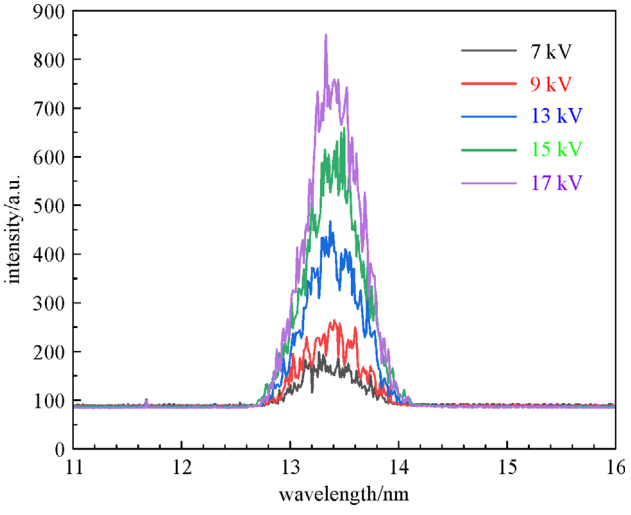

Fig. 7 LPP EUV spectra with different voltages

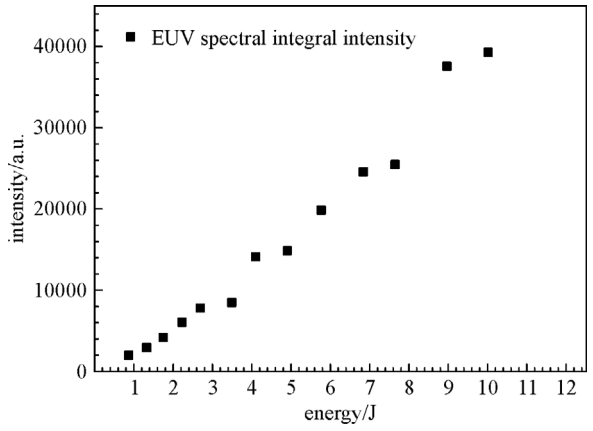

Fig. 8 Relationship between solid Sn EUV spectral intensity and discharge energy

related to the discharge energy. As mentioned above, the higher voltages brought plasmas with higher temperatures and densities and ionized states which were helpful to the emission of EUV.

The conversion efficiency of EUV radiation is roughly estimated. The conversion efficiency (CE) was defined as the ratio of the sum of photon energy Q_{EUV} (with a central wavelength of 13.5 nm and a bandwidth of 2%) to the sum of laser energy Q_{laser} and capacitive storage energy $Q_{\mathrm{discharge}}$, as shown in Eq. (8).

$$\mathrm{CE} = \frac{Q_{\mathrm{EUV}}}{Q_{\mathrm{laser}} + Q_{\mathrm{discharge}}} = \frac{Nhc}{\lambda\eta_1\eta_2\eta_3\eta_4(Q_{\mathrm{laser}} + Q_{\mathrm{discharge}})}, \tag{8}$$

where h was the Planck constant, c was the light speed, η_1 was the product of reflectance of spherical mirror, plane mirror, grating and transmittance of Zr film, η_2 was the first-order diffraction efficiency of grating, η_3 was the acceptance percentage of the spherical mirror, η_4 was the quantum efficiency of CCD and N was total photon number in bandwidth. With the increase of voltage, the EUV CE also improved and the CE was 0.15% when the discharge voltage was 15 kV.

4 Conclusions

In this paper, the solid tin was used to investigate LDP EUV source with different voltages. Under the condition of 145 mJ laser energy and 6 mm gap, we obtained the LDP visible spectra and EUV spectra.

The visible spectra mainly consisted of neutral, singly ionized, and doubly ionized Sn. The intensity of emission lines, electron temperature, electron density and average ionized states all rose with the increase of current and then reduced with the decrease of current. The initial laser

produced plasma had an electron temperature of about 2 eV and a density of about 2×10^{17} cm^{-3}. With the heating of current, the density and temperature of plasma increased further. When the voltage was 15 kV, the highest electron temperature was 6.32 eV at the current peak and the highest electron density was 1.16×10^{18} cm^{-3} a few hundreds of nanoseconds before the current peak.

The plasma radiation was related to the electron temperature. A higher temperature meant more Sn^{7+-13+} ions were produced which helped the 13.5 nm in-band radiation. It was concluded the strongest EUV emission was at the moment of current peak. For the Sn EUV source, the spectra showed a strong peak between 13 and 14 nm when the voltage was higher than 7 kV. With the increase of voltage, the EUV spectral intensity and CE both increased. Increasing the discharge voltage was a simple way to increase the EUV output, but under our current experimental conditions, the current rising rate was a bit slow and the plasma was not concentrated effectively, so the EUV CE and energy utilization were not high enough, it should be improved in our future work.

Acknowledgements This work was supported by the Fundamental Research Funds for the Central Universities (HUST: 2016YXMS028).

References

1. Wagner C, Harned N. Lithography gets extreme. Nature Photonics, 2010, 4(1): 24–26
2. van de Kerkhof M, Jasper H, Levasier L, Peteers R, van Es R, Bosker J, Zdravkov A, Lenderink E, Evangelista F, Broman P, Bilski B, Last T. Enabling sub-10 nm node lithography: presenting the NXE: 3400B EUV scanner. In: Proceedings of SPIE 10143, Extreme Ultraviolet (EUV) Lithography VIII. San Jose: SPIE, 2017, 101430D
3. Meiling H, Buzing N, Cummings K, Harned N, Hultermans B, de Jonge R, Kessels B, Kürz P, Lok S, Lowisch M, Mallman J, Pierson B, Wagner C, van Dijk A, van Setten E, ZimmermSan an J. EUVL system: moving towards production. In: Proceedings of SPIE 7271, Alternative Lithographic Technologies. San Jose: SPIE, 2009, 727102
4. O'Sullivan G, Li B, D'Arcy R, Dunne P, Hayden P, Kilbane D, McCormack T, Ohashi H, O'Reilly F, Sheridan P, Sokell E, Suzuki C, Higashiguchi T. Spectroscopy of highly charged ions and its relevance to EUV and soft X-ray source development. Journal of Physics B, Atomic, Molecular, and Optical Physics, 2015, 48(14): 144025
5. Fomenkov I V, Ershov Al, Partlo W N , Myers D W, Sandstrom R L, Bowering N R, Vaschenko G O, KhodykinO V, Bykanov A N, Srivastava S N, Ahmad I, Rajyaguru C, Golich D J, Dea S D, Hou R r, O'Brien K M, Dunstan W J, Brandt D C. Laser-produced plasma light sources for EUVL. In: Proceedings of SPIE 7636, Extreme Ultraviolet (EUV) Lithography. San Jose: SPIE, 2010, 763639
6. Hotta E, Sakai Y, Hayashi Y, Niimi G, Huang B, Zhu Q S, Song I, Watanabe M. Extreme ultraviolet light sources and soft X-ray laser based on discharge produced plasma. In: Proceedings of SPIE 9524, International Conference on Optical and Photonic Engineering (icOPEN 2015). Singapore: SPIE, 2015, 95242U
7. Stamm U, Kleinschmidt J, Bolshukhin D, Brudermann J, Hergenhan G, Korobotchko V, Nikolaus B, Schürmann M C, Schriever G, Ziener C, Borisov V M. Development status of EUV sources for use in beta-tools and high-volume chip manufacturing tools. In: Proceedings of SPIE 6151. Emerging Lithographic Technologies X. San Jose: SPIE, 2006, 61510O
8. Beyene G A, Tobin I, Juschkin L, Hayden P, O'Sullivan G, Sokell E, Zakharov V S, Zakharov S V, O'Reilly F. Laser-assisted vacuum arc extreme ultraviolet source: a comparison of picosecond and nanosecond laser triggering. Journal of Physics D, Applied Physics, 2016, 49(22): 225201
9. Schriever G, Semprez O, Jonkers J, Yoshioka M, Apetz R. Laser-produced plasma versus laser-assisted discharge plasma: physics and technology of extreme ultraviolet lithography light sources. Journal of Micro/Nanolithography, MEMS, and MOEMS, 2012, 11 (2): 021104
10. Teramoto Y, Narihiro Z, Yamatani D, Yokoyama T, Bessho K, Joshima Y. Development of Sn-fueled high-power DPP EUV source for enabling HVM. In: Proceedings of SPIE 6517, Emerging Lithographic Technologies XI. San Jose: SPIE, 2007, 65173R
11. Teramoto Y, Santos B, Mertens G, Kops R. High-radiance LDP source: clean, reliable, and stable EUV source for mask inspection. In: Proceedings of SPIE 9776, Extreme Ultraviolet (EUV) Lithography VII. San Jose: SPIE, 2016, 97760L
12. Tobin I, Juschkin L, Sidelnikov Y, O'Reilly F, Sheridan P, Sokell E, Lunney J G. Laser triggered Z-pinch broadband extreme ultraviolet source for metrology. Applied Physics Letters, 2013, 102(20): 203504
13. Turkot B, Carson S L, Lio A, Liang T, Phillips M, McCool B, Stenehjem E, Crimmins T, Zhang G J, Sivakumar S. EUV progress toward HVM readiness. In: Proceedings of SPIE 9776, Extreme Ultraviolet (EUV) Lithography VII. San Jose: SPIE, 2016, 977602
14. Teramoto Y, Santos B, Mertens G, Kops R. High-radiance LDP source for mask inspection application. In: Proceedings of SPIE 9048, Extreme Ultraviolet (EUV) Lithography V. San Jose: SPIE, 2014, 904813
15. Teramoto Y, Santos B, Mertens G, Kops R, Kops M, von Wezyk A, Bergmann K, Yabuta H, Nagano A, Ashizawa N, Taniguchi Y, Yamatani D, Shirai T, Kasama K. High-radiance LDP source for mask inspection and beam line applications. In: Proceedings of SPIE 10143, Extreme Ultraviolet (EUV) Lithography VIII. San Jose: SPIE, 2017, 101431L
16. Shaikh N M, Tao Y, Burdt R A, Yuspeh S, Amin N, Tillack M S. Spectroscopic analysis of temperature and density of Sn plasma produced by a CO_2 laser. Journal of Applied Physics, 2010, 108(8): 083109
17. Wu T, Wang X, Zuo D, Lu P. Research of pulse CO2 laser produced tin plasma. In: Proceedings of SPIE 8603, High-Power Laser Materials Processing: Lasers, Beam Delivery, Diagnostics, and Applications II. San Francisco: SPIE, 2013, 86030Y
18. Kieft E R, van der Mullen J, Kroesen G M W, Banine V, Koshelev K N. Stark broadening experiments on a vacuum arc discharge in tin vapor. Physical Review E: Statistical, Nonlinear, and Soft Matter

Physics, 2004, 70(6): 066402
19. Kieft E R, van der Mullen J, Kroesen G M W, Banine V, Koshelev K N. Characterization of a vacuum-arc discharge in tin vapor using time-resolved plasma imaging and extreme ultraviolet spectrometry. Physical Review E: Statistical, Nonlinear, and Soft Matter Physics, 2005, 71(2): 026409
20. Zhu Q, Muto T, Yamada J, Kishi N, Watanabe M, Okino A, Horioka K, Hotta E. Estimation of electron temperature and density of the decay plasma in a laser-assisted discharge plasma extreme ultraviolet source by using a modified Stark broadening method. Journal of Applied Physics, 2011, 110(12): 123302
21. Tobin I. Optical and EUV studied of laser triggered Z-pinch discharges. Dissertation for the Doctoral. Dublin, Ireland: Trinity College, 2014, 20–300
22. Djeniže S, Srećković A, Nikolić Z. On the Sn I and Sn II Stark broadening. Journal of Physics B, Atomic, Molecular, and Optical Physics, 2006, 39(14): 3037–3045
23. Griem H R. Semiempirical formulas for the electron-impact widths and shifts of isolated ion lines in plasmas. Physical Review, 1968, 165(1): 258–266
24. Aydin Ü, Roth P, Gehlen C D, Noll R. Spectral line selection for time-resolved investigations of laser-induced plasmas by an iterative Boltzmann plot method. Spectrochimica Acta Part B, Atomic Spectroscopy, 2008, 63(10): 1060–1065
25. Miller M H, Roig R A, Bengtson R D. Experimental transition probabilities and Stark-broadening parameters of neutral and singly ionized tin. Physical Review A, 1979, 20(2): 499–506
26. Coons R W, Harilal S S, Polek M, Hassanein A. Spatial and temporal variations of electron temperatures and densities from EUV-emitting lithium plasmas. Analytical and Bioanalytical Chemistry, 2011, 400(10): 3239–3246
27. Zhu Q, Yamada J, Kishi N, Hosokai T, Watanabe M, Okino A, Horioka K, Hotta E. Pinch dynamics of the 13.5 nm EUV-emitting plasma in a LA-DPP source. In: Proceedings of 2011 Academic International Symposium on Optoelectronics and Microelectronics Technology. Haerbin, 2011, 172–175
28. Zhang J, Gu P J. An approximate method for calculating ionization state of local thermodynamic equilibrium and nonlocal thermodynamic equilibrium plasma. Chinese Journal of Computational Physics, 1987, 4(1): 1–16 (in Chinese)

Junwu WANG, Ph.D., Huazhong University of Science and Technology (HUST). He received the Bachelor degree in Optical Engineering from School of Optical and Electronic Information, HUST in 2014. He is studying for his Ph.D. degree in Wuhan National Laboratory for Optoelectronics, HUST. His main research is laser induced discharge produced plasma EUV source.

Xinbing WANG, professor, Huazhong University of Science and Technology, Wuhan China. He received the Bachelor and Master degrees in Engineering from South East University, Nanjing, China, and Ph.D. degree from Huazhong University of Science and Technology in Physical Electronics in 1997. Now he is working in the Wuhan National Laboratory for Optoelectronics as a professor. His main research is laser produced plasma EUV source.

Duluo ZUO, Ph.D., and Professor of Optical Engineering of Wuhan National Laboratory of Optoelectronics, Huazhong University of Science and Technology (HUST). He got his Bachelor degree in Laser Technology from HUST in 1987, his Master and Ph.D. degrees in Optics from Anhui Institute of Optics and Fine Mechanics in 1990 and 1993. He has been employed by HUST since 1994, mainly engaged in the researches on high power lasers and their applications, such as high power fast axial flow CO_2 laser, high energy TEA CO_2 laser, laser propulsion, excimer laser and laser-produced plasma light source for microlithography, as well as laser spectroscopy of Raman scattering and its application in gas analysis. Now his main research topics are laser spectroscopy in gas analysis, optically pumped noble gas lasers, and laser-produced plasma source.